Available online at www.sciencedirect.com

SciVerse ScienceDirect

journal homepage: www.elsevier.com/locate/he

Stability of transition metals on Mg(0001) surfaces and their effects on hydrogen adsorption

Ming Chen [a], *Xiao-Bao Yang* [a], *Jie Cui* [b], *Jia-Jun Tang* [a], *Li-Yong Gan* [a], *Min Zhu* [b], *Yu-Jun Zhao* [a,*]

[a] *Department of Physics, South China University of Technology, Guangzhou 510640, People's Republic of China*
[b] *School of Material Science and Engineering, South China University of Technology, Guangzhou 510640, People's Republic of China*

ARTICLE INFO

Article history:
Received 21 May 2011
Received in revised form
4 September 2011
Accepted 16 September 2011
Available online 13 October 2011

Keywords:
Hydrogen storage
Magnesium
Transition metal doping
ab initio calculation

ABSTRACT

The interactions of a hydrogen atom with clean, vacancied, and transition metal-doped (TM = Sc, Ti, V, Cr, Mn, Fe, Co, Ni, Cu, Zn, Y, Zr, Nb, Mo, Tc, Ru, Rh, Pd, Ag, Cd, Au, Pt) Mg(0001) surfaces are investigated using first-principles calculations. The H adsorption on Mg(0001) with TMs doped within the second layer is generally more stable than that on clean Mg but clearly weaker than that on Mg surfaces with TM in the first layer. We find, however, that all these TM atoms prefer to substitute for the Mg atoms in the second layer rather than for those in the outermost layer of the Mg surface. To enhance the catalytic effect of the TM dopants, we investigated various co-doping conditions of TMs, and we found that i) Ti is a good "assistant" that stabilizes co-doped Co, Ni, Pd, Ag, Pt, and Au within the first layers and that ii) Ni and Co are more easily incorporated into the first layer of a Mg surface when co-doped with Ti, V, and Nb. These observations may lead to a possible approach to stabilize the TM dopants within the first layer and thus promote the hydrogenation of Mg accordingly.

1. Introduction

To avoid a fossil fuel-dependent energy crisis and an undesirable climate change, the development of new means of clean and sustainable energy has attracted wide attention worldwide [1]. Hydrogen, if it can be produced from renewable sources and utilized conveniently, would undoubtedly be a phenomenal choice because it has a high energy density and is pollution free. However, the storage of hydrogen fuel in an economical and convenient manner presents a bottle-neck in the practical application of hydrogen fuel. MgH_2 is a hydrogen storage material with the potential to overcome this bottle-neck, which has a gravimetric storage capacity of 7.6% and a relatively low cost [2]. However, two serious limitations exist for MgH_2. The first limitation of MgH_2 is its hydride stability; the release of hydrogen from MgH_2 occurs at temperatures in excess of 300 °C at 1 bar H_2 because a phase transformation from ionic MgH_2 to hcp metal Mg with interstitial H is required during dehydrogenation [3]. The second limitation of MgH_2 is its slow kinetics of dehydrogenation and hydrogenation [4], which has mainly been ascribed to i) a resistance to hydrogenation by the oxide layer covering the surface of the Mg particle [5], ii) a poor dissociation rate for hydrogen at the Mg surface [6], or iii) a slow diffusion rate for hydrogen in MgH_2 [7,8].

A common and effective way to overcome these limitations in MgH_2 is ball milling, which can lead to faster kinetics due to the shortening of diffusion length scales, the increasing

* *Corresponding author*. Tel: +86 20 87110426; fax: +86 20 87112837.
E-mail addresses: zhaoyj@scut.edu.cn, 624816914@qq.com (Y.-J. Zhao).
0360-3199/$ – see front matter Copyright © 2011, Hydrogen Energy Publications, LLC. Published by Elsevier Ltd. All rights reserved.
doi:10.1016/j.ijhydene.2011.09.065

of the surface area and the introduction of defects [9]. It has also been observed that nanoscaling of MgH_2 can improve its thermodynamic behavior [10]. However, scaling up the size of nanoparticles is not straightforward for commercial applications because the process is complicated and energy intensive [8].

An alternative way to overcome the limitations of MgH_2 is to dope transition metals (TMs) into the material. This doping is expected to weaken the Mg–H bond and reduce the stability of the hydride. Liang et al. investigated the catalytic effects of five 3d elements (Ti, V, Mn, Fe and Ni) on the reaction kinetics of MgH_2 by monitoring the rapid desorption at low temperature for MgH_2–TM and the rapid absorption kinetics for Mg–TM [11]. Zaluska et al. found that the best kinetic results are achieved with a combination of the metals, such as V + Zr or Mn + Zr Mg alloys [10]. Gutfleish et al. investigated Mg alloyed with Ni (1 wt%) and Pd (0.2%) and observed excellent hydrogen absorption/desorption kinetics and cyclic stability of the material, which exhibits an overall reversible H_2 storage capacity of 6.3 wt% [12]. Molinas et al. added a Zr + Ni alloy catalyst to MgH_2 and reported that it absorbed about 5 wt% H_2 in less than 3 min and desorbed the same amount in 7 min at 300 °C [13]. Another promising material is Mg–NiY, which can reach a dehydrogenation rate of up to 1 wt%-H/min at temperatures of 250 °C, and the structure remains nanocrystalline after several cycles [14]. Furthermore, oxides are also reported to improve the kinetics of MgH_2, e.g., Nb_2O_5 [15]. Interestingly, *multiple* oxide additions are generally found to have a more remarkable effect in improving the desorption kinetics of MgH_2 than does a *single* oxide addition [16]. Patah et al. reported that a high hydrogen capacity and fast kinetics were achieved by adding powders of Cr_2O_3 and Nb_2O_5, and the activation energy for the hydrogen desorption was estimated to be ~185 kJ/mol, compared to that of ~206 kJ/mol in MgH_2 [16].

From a theoretical point of view, there are some reports of TMs acting as catalysts for hydrogen absorption on Mg surfaces to improve the kinetics. Du et al. performed calculations on the pure Mg(0001) surface and the Ti-, Pd-, and V-incorporated Mg surfaces [17–19]. Ni- and Ti-doped Mg(0001) surfaces were investigated by Pozzo et al. [20], who reported a systematic theoretical investigation of H_2 dissociation and the subsequent atomic H diffusion on TM (Ti, V, Zr, Fe, Ru, Co, Rh, Ni, Pd, Cu, Ag)-doped Mg(0001) surfaces [21]. Additionally, vacancies are also reported to influence the diffusion barriers [22,23]. However, most of these theoretical studies were based on an assumption that TMs (or vacancies) are located at the outermost layer of Mg. Banerjee et al. reported that Ti, V, and Ni preferred to substitute for one of the Mg atoms within the second layer rather than for one in the top layer; thus, the catalytic effect of these TMs was degraded [24], and co-doping of V and Ti could stabilize Ni in the first layer [25].

For this paper, we conducted a systematic investigation of TM-doped Mg surfaces and their interaction with H atoms. To verify the reliability of these studies, we first employed an *ab initio* method for the calculations of the bulk structural parameters of various elements. By placing the dopant and vacancy in various layers, we investigated both the stability of TM doping and vacancies on the Mg(0001) surfaces and the ability of these surfaces to adsorb hydrogen atoms. We also found that Ni and Co are easily incorporated into the first layer of Mg surfaces when they are co-doped with Ti, V, and Nb and that Ti is a good "assistant" that stabilizes co-doped Co, Ni, Pd, Ag, Pt, and Au within the first layers. Our results may be useful for the design of Mg-based, high-efficiency hydrogen storage media.

Table 1 – Bulk properties of Mg and transition metals (TM = Sc, Ti, V, Cr, Mn, Fe, Co, Ni, Cu, Zn, Y, Zr, Nb, Mo, Tc, Ru, Rh, Pd, Ag, Cd, Au, Pt). For each element, bulk lattice constants (fcc and bcc: *a*; hcp: *a*, *c*) and cohesive energies were calculated and compared to the corresponding experimental data from Ref. [29]. Their atomic radii (*R*) and Pauli electronegativities (X_p) are also listed [44,45].

	STR		*a*, *c*	E_{coh} (eV)	R (Å)	X_p
Mg	hcp	Cal	3.19, 5.19	1.51	1.60	1.31
		Exp	3.21, 5.21	1.51		
Mn	fcc	Cal	3.52	3.78	1.35	1.55
		Exp	3.49	2.92		
Ni	fcc	Cal	3.52	4.87	1.25	1.91
		Exp	3.52	4.44		
Cu	fcc	Cal	3.63	3.48	1.28	1.90
		Exp	3.61	3.49		
Rh	fcc	Cal	3.84	5.92	1.34	2.28
		Exp	3.80	5.75		
Pd	fcc	Cal	3.95	3.70	1.38	2.20
		Exp	3.89	3.89		
Ag	fcc	Cal	4.15	2.48	1.44	1.93
		Exp	4.08	2.95		
Pt	fcc	Cal	3.98	5.53	1.38	2.28
		Exp	3.92	5.84		
Au	fcc	Cal	4.17	2.98	1.44	2.54
		Exp	4.08	3.81		
V	bcc	Cal	2.98	5.40	1.35	1.63
		Exp	3.03	5.31		
Cr	bcc	Cal	2.84	4.03	1.3	1.66
		Exp	2.88	4.10		
Fe	bcc	Cal	2.83	4.94	1.26	1.83
		Exp	2.87	4.28		
Nb	bcc	Cal	3.30	7.01	1.41	1.60
		Exp	3.30	7.57		
Mo	bcc	Cal	3.15	6.37	1.36	2.16
		Exp	3.15	6.82		
Sc	hcp	Cal	3.32, 5.16	4.15	1.64	1.36
		Exp	3.31, 5.27	3.90		
Ti	hcp	Cal	2.92, 4.63	5.47	1.47	1.54
		Exp	2.95, 4.68	4.85		
Co	hcp	Cal	2.49, 4.04	5.30	1.25	1.88
		Exp	2.51, 4.07	4.39		
Zn	hcp	Cal	2.70, 5.00	1.08	1.37	1.65
		Exp	2.66, 4.95	1.35		
Y	hcp	Cal	3.65, 5.67	4.30	1.80	1.22
		Exp	3.65, 5.73	4.37		
Zr	hcp	Cal	3.24, 5.16	6.37	1.57	1.33
		Exp	3.23, 5.15	6.25		
Tc	hcp	Cal	2.75, 4.41	6.85	1.30	1.90
		Exp	2.74, 4.40	6.85		
Ru	hcp	Cal	2.72, 4.30	7.48	1.33	2.20
		Exp	2.71, 4.28	6.74		
Cd	hcp	Cal	3.02, 5.66	0.72	1.49	1.69
		Exp	2.98, 5.62	1.16		

2. Computational method

Our calculations were performed with the *ab initio* simulation package VASP [26]. The Perdew–Burke–Ernzerhof functional was used for the calculation of the exchange-correlation energy [27]. The electron–ion interactions were described by the projector augmented wave (PAW) method [28]. For all calculations, the plane wave cutoff energy was set at 400 eV. For all of the relaxations, an energy difference of 10^{-4} eV was set as the convergence criterion between successive ionic steps.

The optimized lattice constants of bulk Mg were $a = 3.19$ Å and $c = 5.19$ Å, and the cohesive energy (E_{coh}) was 1.51 eV/atom in our calculations, all of which are in agreement with the experimental values ($a = 3.21$ Å, $c = 5.21$ Å, $E_{coh} = 1.51$ eV/atom) [29,30]. The clean, single-vacancied, and single-TM-doped Mg(0001) surfaces were modeled by a five-layer 3×3 slab, whereas the surfaces of pair-doped Mg(0001) surfaces were modeled by a five-layer 3×5 slab. Monkhorst-Pack grids of $(5 \times 5 \times 1)$ and $(1 \times 1 \times 1)$ were used in the Brillouin zone sampling [31] for the 3×3 and 3×5 slabs, respectively. The top three layers in each slab were fully relaxed in the calculations, whereas the bottom two layers were fixed at their bulk configurations. The vacuum space was set to 15 Å to guarantee a sufficient separation between the periodic images. The stability of pair TMs on the 3×5 slab were tested for (V, Ni), (V, Co), (Nb, Ni), (Nb, Co) with Monkhorst-Pack grids of $(5 \times 5 \times 1)$, and we found that the relative stability of various configurations (1st layer vs. 2nd layer) were unchanged, though the absolute energy difference was increased to 0.1 eV. The analyses of the charge transfer and charge density difference were based on the Bader charge allocation [32,33].

3. Results and discussion

3.1. Stability of TMs and vacancies on the Mg(0001) surface

We have studied the stability of vacancy and TM substitutions in different layers of Mg surfaces. The TM doping at the interstitial sites is not considered because it has been reported that it is not energetically preferable [24]. The substitutional energy (E_{sub}) for TM-doped and vacancy-doped surfaces is defined as:

$$E_{sub} = E_{M/Mg(0001)} + E_{Mg} - E_{M} - E_{Mg(0001)} \quad (1)$$

where $E_{M/Mg(0001)}$ is the energy of the TM-substituted Mg surface, E_{Mg} is the energy of the Mg in the bulk structure, E_M is the energy of the TM in its bulk structure (zero for a vacancy), and $E_{Mg(0001)}$ is the energy of a clean Mg surface. By definition, a negative E_{sub} value implies that the TM is not expected to segregate because it prefers to be surrounded by Mg atoms over its pure bulk state. The structural parameters, the cohesive energies of the TMs and Mg, and the atomic radii and electronegativities are listed in Appendix and in Table 1.

The calculated E_{sub} values for various TMs, arranged by the TM's atomic number, as well as those for the vacancy Mg at

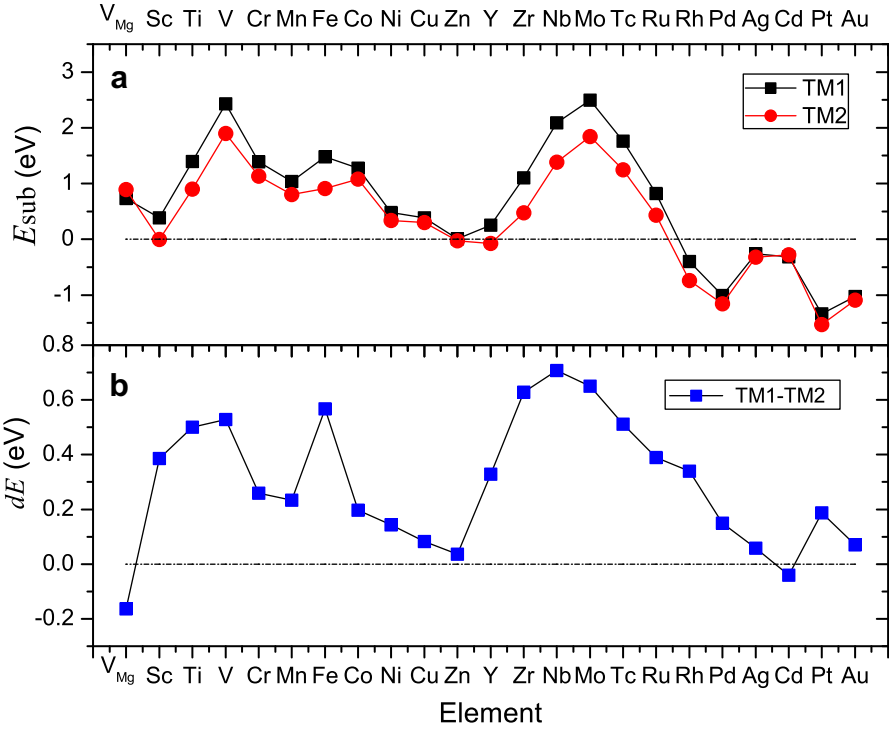

Fig. 1 – (a) The substitutional energies of transition metals (vacancy for Mg). Black represents TMs doped in the first layer, and red represents TMs doped in the second layer. (b) The differences between the substitutional energies of TMs doped in the first layer and those of TMs doped in the second layer. Positive values indicate a preference for the second layers (For interpretation of the references to color in this figure legend, the reader is referred to the web version of this article.)

the first and second layers of the Mg surface are illustrated in Fig. 1. We found that the vacancy prefers to be in the outermost layer rather than in the second layer because it has a lower coordination number in the outermost layer. The E_{sub} value at the first and second layers increases from Sc to V and from Y to Mo, whereas this value generally decreases from V to Zn and from Mo to Pd. According to the energy difference (dE) shown in Fig. 1(b), it is clear that all of the studied TMs prefer to stay in the second layer, but the vacancy Mg prefers to be in the first layer. The substitutional energies of all of the TMs except Rh, Pd, Ag, Cd, Pt, and Au are positive, indicating a tendency to segregate for most of TMs. In fact, Nb atoms were reported experimentally to form a cluster in Nb-doped magnesium hydride when the Nb concentration is greater than 5 at.%, though the clustering is negligible when its concentration is lower than 1 at.% [34].

The local structural distortions that are introduced by the substitution of TM atoms were also investigated by comparison to the clean surface. As shown in Fig. 2(a), when a TM substitutes for Mg in the first layer, all the TMs except Y are contracted toward the bulk, forming dips on surface. It would be difficult for Y atoms to diffuse from the first layer into the bulk because the radius of Y is significantly larger than that of Mg (c.f. Table 1). As shown in Fig. 2(a), there is a nonmonotonic trend in the distortions as the atomic number of the TM increases. Sc and Y experience outward distortions, whereas Co, Ni, Ru, Pd, and Au exhibit inward-directed distortions. When a TM substitutes for Mg in the second layer, three scenarios are observed: (1) Sc, Ti, V, Y, Zr, and Nb distort slightly out of the surface with respect to the ideal lattice sites; (2) Fe and Mo exhibit no significant dislocation; and (3) other TMs are clearly shifted inward relative to the bulk structure.

In general, the interaction between a TM and Mg is dominated by the d levels of the TM and the p levels of Mg. In our studies, we found that the distortion of the TM in the Mg surface is consistent with the radius and the relative electronegativity of the TM (c.f. Fig. 2). From the dislocations and radii shown in Fig. 2, we noticed that TMs with smaller radii experience more significant inward shifts relative to the bulk structure. Fig. 2(c) shows the charge transfer between the dopant atoms and the Mg surface, which were obtained through a Bader charge analysis. The positive values indicate a charge transfer from the TM surface to the Mg, whereas the direction of this transfer is reversed for the negative values. As shown in Fig. 2(c), the trend of charge transfer between the TM and the Mg surface is also related to the distortion shown in Fig. 2(a), indicating the significance of electronegativity effects on the distortion.

Fig. 3 shows the charge density difference of some selected TM-doped (Cr, Ni, Y, and Nb) Mg surfaces. Here,

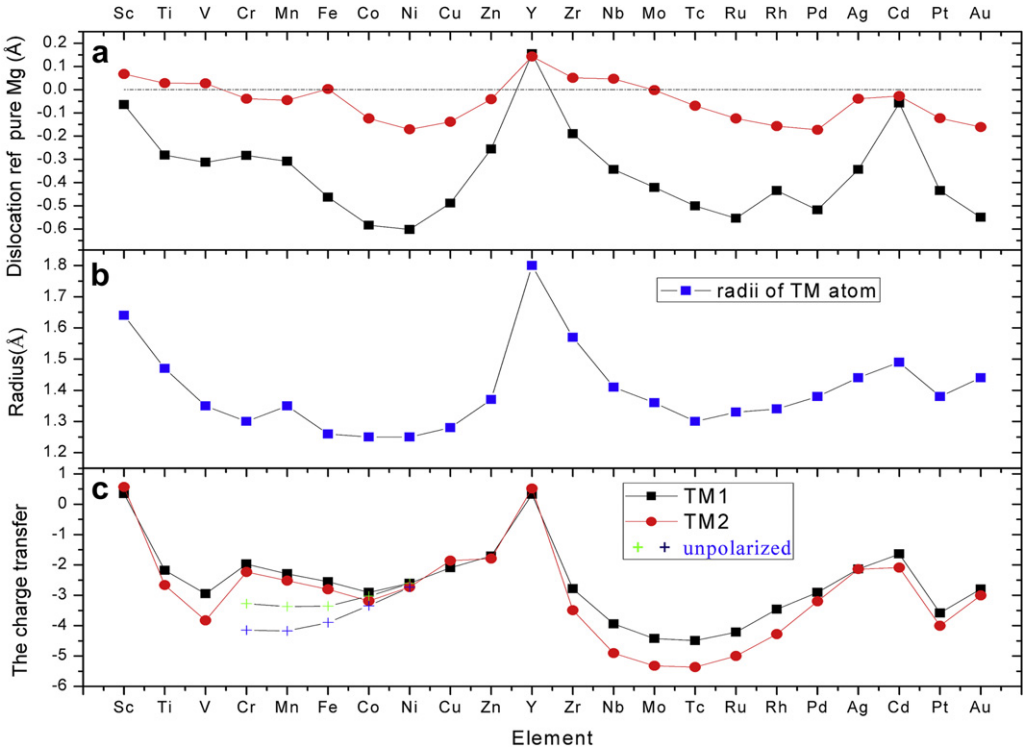

Fig. 2 – (a) The dislocation of the TM with respect to the substituted Mg position on the pure Mg surface. Black and red symbols represent the TM doped in the first layer and second layer, respectively. We calculated the distortions with the following equation: $d_z = z_M - z_{Mg}$, where z_M is the height of the TM and z_{Mg} is the height of the corresponding Mg before the substitution. (b) The radii of the related elements. (c) Charge transfers between the doped metal atom (black and red corresponding to the first and second layers, respectively) and the Mg surface. Positive values indicate that the charge transfer occurs from the metal atom to Mg. The blue (green) crosses represent unpolarized Cr, Mn, Fe, and Ni atoms in the second (first) layer (For interpretation of the references to color in this figure legend, the reader is referred to the web version of this article.)

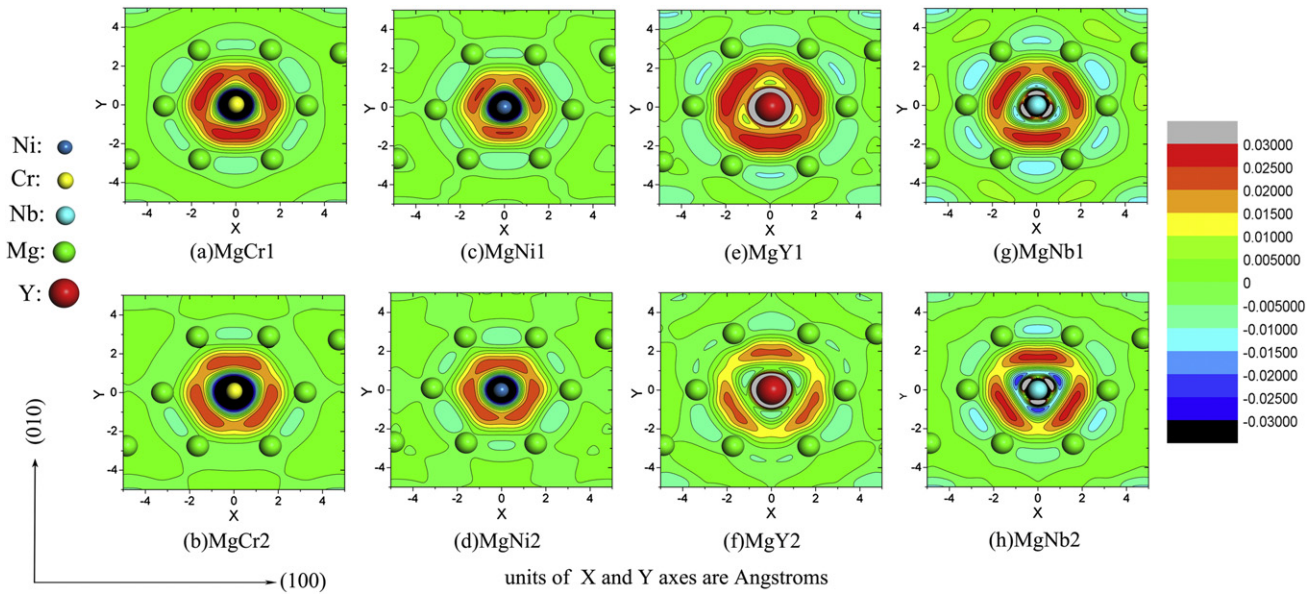

Fig. 3 – Charge density difference distributions on (0001) crystal planes of the selected Mg surface structures alloyed with Cr, Ni, Y, and Nb. MgCr1, MgNi1, MgY1, and MgNb1 represent Cr, Ni, Y, and Nb doped in the first layer. MgCr2, MgNi2, MgY2, and MgNb2 represent Cr, Ni, Y, and Nb doped in the second layer.

$\rho_{diff} = \rho_{Mg/TM} - \rho_{Mg} - \rho_{TM}$, where $\rho_{Mg/TM}$, ρ_{Mg}, and ρ_{TM} stand for the charges corresponding to the TM-doped Mg(0001) surface, the TM-doped Mg(0001) surface with the TM atom removed, and the free TM atom, respectively. For Cr, Ni, and Nb, the charge transferred from the six nearest-neighbor Mg atoms around the doped atom is accumulated on the doped atoms because their electronegativities are more negative than that of Mg. However, there is charge transferred from Y to the Mg atoms due to Y's less negative electronegativity. The charges are accumulated in the region between the doped atom and its nearest-neighbor Mg atoms as shown in Fig. 3(e) and (f).

3.2. *Interactions of hydrogen atoms with clean and TM-doped Mg(0001) surfaces*

In the following discussion, we consider the interaction between the hydrogen atom, the clean Mg surface, and the doped TM in the first or the second Mg layer. Here, only the three-fold sites, as well as the top sites for a comparison (as indicated in Fig. 4), are investigated for the hydrogen adsorption because it was clear that H prefers the three-fold sites on a clean Mg(0001) surface [20]. The adsorption energies ($E_{ads(H)}$) for the hydrogen atom are defined as:

$$E_{ads(H)} = E_{slab(Mg-M-H)} - E_{slab(Mg-M)} - (1/2)E_{H_2} \quad (2)$$

where $E_{slab(Mg-M-H)}$ is the energy of a slab with one H adsorbed on the surface, $E_{slab(Mg-M)}$ is the energy of a TM-doped slab without H, and is the energy of a isolated hydrogen molecule.

It was found that the hydrogen atoms at the three-fold sites are much more stable than those at the corresponding top sites. We focus on the most stable adsorption configurations with the most negative $E_{ad(H)}$. As shown in Fig. 5, on most of the first-layer TM-doped Mg(0001) surfaces, $E_{ad(H)}$ is significantly lowered by ~0.5 eV relative to that of the clean Mg surface. However, this is not the case for Zn-, Ag-, Cd-, and Au-doped surfaces, on which H adsorption is even weaker, or Cu-, Pd-, Pt-doped surfaces, on which $E_{ad(H)}$ is lowered by 0.1–0.2 eV, which is less significant than that of other H adsorption-enhanced TMs. Of note, in the above exceptions, the doping TMs have fully or nearly fully filled d levels. In general, for surfaces with TMs doped in the first layer, $E_{ad(H)}$ values for the surfaces doped with TMs on the left of the periodic table are strong, whereas $E_{ad(H)}$ values are weak for the TMs on the right of the periodic table. This observation agrees well with the results reported by Pozzo et al. that suggest that both the doping effect of TMs on the dissociation barrier of H_2 and the ability of TM-doped surfaces to bind H atoms depends on the positions of the TMs in the periodic table [21]. Alternatively, when the TM is located in the second layer, the H adsorption energy of any TM-doped surface has

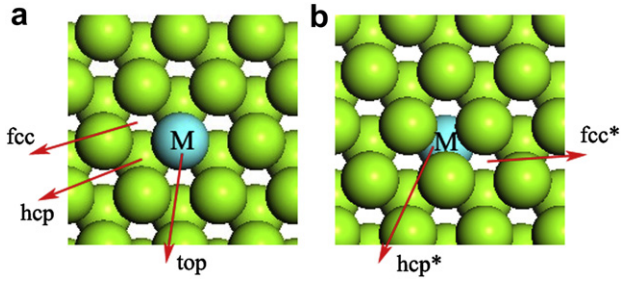

Fig. 4 – Top view of possible sites for a hydrogen atom in the first (a) and second (b) layers. The blue sphere (M) represents the doped TM or vacancy, and green spheres represent Mg (For interpretation of the references to color in this figure legend, the reader is referred to the web version of this article.)

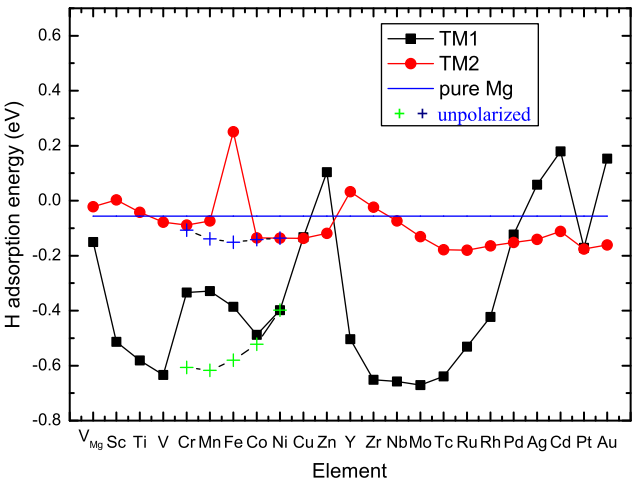

Fig. 5 – The hydrogen adsorption energies of various TM-doped Mg surfaces. Black squares correspond to a TM doped in the first layer of a Mg(0001) surface, whereas the red circles correspond to a TM in the second layer. The blue (green) crosses represent unpolarized Cr, Mn, Fe, and Ni atoms in the second (first) layer (For interpretation of the references to color in this figure legend, the reader is referred to the web version of this article.)

no significant change (typically within 0.2 eV) relative to those of a pure Mg surface, which indicates that it is necessary to retain the TMs in the outermost layer of the Mg(0001) surface to enhance the adsorption of H.

Compared to the pure Mg(0001) surface, H is less stable on the surfaces with Zn, Ag, Cd, and Au located in the outermost layer (c.f. Fig. 5). This observation agrees well with the experimentally reported hydrogen desorption temperatures on Ag(110), Ag(111), and Au(111) surfaces, which are 155–175 K [35], 180 K [36], and 110 K [37], respectively, lower than the 573 K [2] observed for the Mg surface. The mechanically alloyed pure Mg–Cd alloys are very difficult to activate for hydrogen absorption [38]. Interestingly, for Zn, Ag, Cd, and Au, H is more stable on the surfaces with those TMs in the second layer than in the first layer. This fact can be attributed to the surface distortion induced by the TMs doped in the second layer, which is beneficial to hydrogen adsorption [15]. It is noticeable that the H adsorption energies on the Mn- and Fe-doped surfaces are irregular with respect to the adjacent elements (c.f. Fig. 5). This observation is attributed to the spin polarization effect because the irregularity disappears when we eliminate the effects of spin polarization for Cr-, Mn-, and Fe-doped systems, as shown in Fig. 5. The spin polarization has little impact on the H adsorption of Co- and Ni-doped surfaces because the adsorption energy has little change in the absence of spin polarization. This phenomenon is consistent with the charge transfer influenced by the spin polarization [as illustrated in Fig. 2(c)] and indicates that spin polarization treatment is necessary for H adsorption on Cr-, Mn-, and Fe-doped Mg(0001) systems but not for the Co- and Ni-doped systems, in agreement with Refs. [21,39].

3.3. *The stability of co-doped TMs*

Although doped metals in the second layer of Mg surfaces are energetically preferable, their catalytic effects on H adsorption are significantly reduced. It is crucial to stabilize the doped metals at the outermost layer of the Mg surface to enhance their catalytic effect. In the literature, it has been reported that Ni can be stabilized in the first layer when co-doped with V [25]. To stabilize a TM atom B at the outermost layer by co-doping with a second layer atom A, i.e., in the configuration A^2B^1, the following two prerequisites exist. First, the difference in substitutional energy of atom B between the first and second layers should be small enough to be overcome by atom

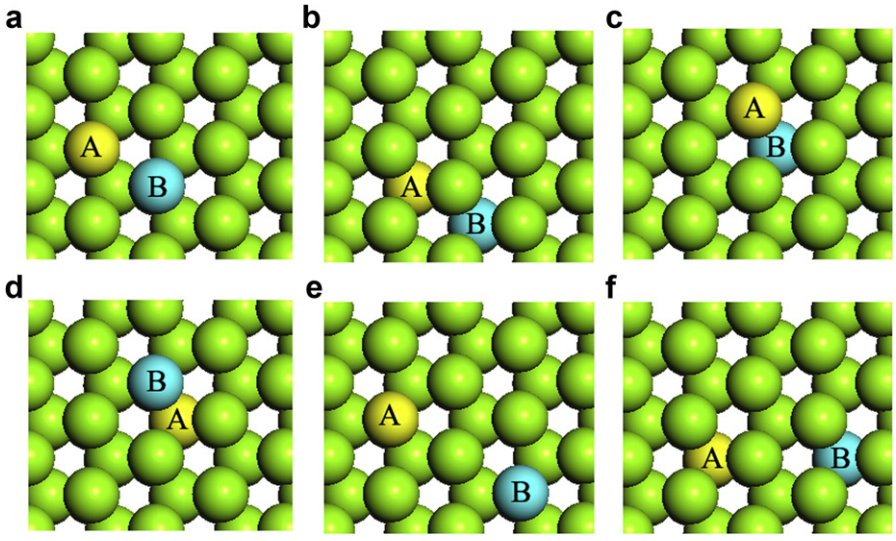

Fig. 6 – Top views of possible configurations of co-doped Mg(0001) surfaces. The green spheres represent Mg atoms, the yellow spheres (A) represent V or Nb, and the blue spheres (B) represent the other co-doped elements. Configurations (a)–(f) correspond to A^1B^1, A^2B^2, A^1B^2, A^2B^1, $(A^1B^1)^*$, $(A^2B^2)^*$, where 1 and 2 refer to the first and second layer in Table 2, respectively (For interpretation of the references to color in this figure legend, the reader is referred to the web version of this article.)

Table 2 – The calculated substitutional energies of various configurations of Sc, Ti, V, Y, Zr and Nb co-doped with Fe, Co, Ni, Cu, Zn, Pd, Ag, Pt, and Au. The detailed structure of configurations A^1B^1, A^2B^2, A^1B^2, A^2B^1, $(A^1B^1)^*$ and $(A^2B^2)^*$ are illustrated in Fig. 6. The substitutional energies of A^2B^1 are displayed in bold when A^2B^1 configuration is favored.

Elements	Substitutional energy (eV)					
	Adjacent				Not adjacent	
	A^1B^1	A^2B^2	A^1B^2	A^2B^1	$(A^1B^1)^*$	$(A^2B^2)^*$
ScFe	1.467	1.157	1.132	**0.967**	1.693	1.010
ScCo	1.067	0.529	0.701	0.612	1.552	0.850
ScNi	0.460	−0.034	0.153	−0.001	0.759	0.160
ScCu	0.580	0.098	0.383	0.127	0.710	0.167
ScZn	0.248	−0.180	0.188	−0.135	0.372	−0.094
ScPd	−0.957	−1.449	−1.210	−1.371	−0.772	−1.387
ScAg	−0.049	−0.509	−0.154	−0.493	0.016	−0.509
ScCd	−0.068	−0.413	−0.013	**−0.461**	−0.002	−0.384
ScPt	−1.453	−1.914	−1.746	−1.834	−1.115	−1.714
ScAu	−0.927	−1.318	−1.057	−1.303	−0.733	−1.236
TiFe	2.469	1.91	2.056	2.311	4.228	2.881
TiCo	2.589	1.99	2.177	**1.93**	3.433	2.766
TiNi	2.307	1.684	1.959	**1.639**	2.709	2.024
TiCu	2.482	1.924	2.332	1.947	2.672	2.068
TiZn	2.184	1.703	2.080	1.709	2.353	1.838
TiPd	1.065	0.421	0.758	0.473	1.182	0.513
TiAg	1.962	1.412	1.856	**1.411**	1.962	1.390
TiCd	0.914	0.505	0.964	**0.441**	0.970	0.511
TiPt	0.541	−0.015	0.140	**−0.033**	0.874	0.162
TiAu	1.127	0.634	0.964	**0.627**	1.255	0.675
VFe	2.469	1.91	2.056	2.311	4.228	2.881
VCo	2.589	1.99	2.177	**1.93**	3.433	2.766
VNi	2.307	1.684	1.959	**1.639**	2.709	2.024
VCu	2.482	1.924	2.332	1.947	2.672	2.068
VZn	2.184	1.703	2.080	1.709	2.353	1.838
VPd	1.065	0.421	0.758	0.473	1.182	0.513
VAg	1.962	1.412	1.856	**1.411**	1.962	1.390
VCd	1.904	1.538	1.962	**1.464**	1.939	1.534
VPt	0.541	−0.015	0.140	**−0.033**	0.874	0.162
VAu	1.127	0.634	0.964	**0.627**	1.255	0.675
YFe	1.374	0.719	1.040	0.950	2.072	0.838
YCo	0.970	0.405	0.622	0.638	1.342	0.606
YNi	0.271	−0.241	−0.022	−0.058	0.573	−0.100
YCu	0.414	−0.119	0.193	−0.024	0.556	−0.023
YZn	0.098	−0.318	0.020	−0.302	0.252	−0.252
YPd	−1.150	−1.692	−1.390	−1.464	−0.953	−1.604
ZrCd	0.569	0.042	0.616	**−0.027**	0.632	0.046
YAg	−0.193	−0.723	−0.314	−0.646	−0.138	−0.682
YCd	−0.216	−0.570	−0.152	**−0.624**	−0.136	−0.539
YPt	−1.662	−2.141	−1.925	−1.888	−1.299	−1.991
YAu	−1.099	−1.540	−1.236	−1.443	−0.882	−1.430
ZrFe	1.799	1.017	1.354	1.050	2.915	1.448
ZrCo	1.500	0.712	0.990	0.734	2.183	1.807
ZrNi	1.062	0.265	0.572	0.263	1.402	0.518
ZrCu	1.233	0.468	0.914	0.485	1.354	0.575
ZrZn	0.856	0.247	0.746	**0.245**	1.040	0.347
ZrPd	−0.244	−1.065	−0.686	−1.000	−0.137	−1.005
ZrAg	0.657	−0.097	0.457	−0.084	0.644	−0.102
ZrPt	−0.804	−1.547	−1.303	−1.480	−0.458	−1.356
ZrAu	−0.223	−0.898	−0.898	−0.887	−0.073	−0.829
NbFe	2.540	1.799	2.069	1.929	3.276	2.317
NbCo	2.339	1.59	1.831	**1.506**	3.042	2.205
NbNi	1.918	1.167	1.533	**1.118**	2.315	1.432
NbCu	2.121	1.368	1.9	1.375	2.280	1.474
NbZn	1.791	1.131	1.675	**1.102**	1.975	1.250
NbPd	0.724	−0.079	0.366	−0.046	0.777	−0.086
NbAg	1.609	0.851	1.484	0.852	1.566	0.796
NbCd	1.535	0.970	1.593	**0.881**	1.561	0.947
NbPt	0.202	−0.575	−0.262	−0.524	0.471	−0.434
NbAu	0.774	0.080	0.576	0.081	0.861	0.082

B's interaction with the "assistant" atom A. According to Fig. 1(b), Co, Ni, Cu, Zn, Pd, Ag, Cd, Pt, and Au fit this criterion (Group B, see below) if we set the energy difference to be within 0.2 eV, though Zn, Ag, and Au in the first layer are not preferred for enhanced H adsorption. Second, the interaction between A^2 and B^1 should be stronger than that between A^2 and B^2 to favor the configuration A^2B^1. In the literature, the remarkable catalytic effects of V and Nb are well supported when these TMs are co-doped with other elements [15,40]. As shown in Fig. 2(a), we observed that both V and Nb are slightly outside the first layer when they are located in the second layer, whereas most of the TMs shift inward relative to the bulk structure. This difference could be beneficial to the interaction of these TMs with other dopants in the first layer and could render them as "assistant" atoms to stabilize other TMs in the first layer. In this work, Sc, Ti, Y, Zr, V, and Nb (Group A, see below), whose second layer distortions are all directed toward the outermost layer [c.f. Fig. 2(b)], were chosen to be co-doped with Group A TMs that were selected according to the above prerequisites, to study the co-doping stability of TMs. In addition, Fe co-doped with Group A atoms was also studied as a comparison.

The stability of the configurations was analyzed by the substitutional energy defined as:

$$E = E_{AB/Mg(0001)} + 2E_{Mg}^{atom} - E_A - E_B - E_{Mg(0001)} \quad (3)$$

where $E_{AB/Mg(0001)}$ is the energy of the A- and B-substituted Mg(0001) surface, E_{Mg}^{atom} and E_A (E_B) are the energies of each atom in their corresponding bulk structures.

Several possible configurations of the two impurities are considered in the calculations, including the adjacent configurations A^1B^1, A^1B^2, A^2B^1, and A^2B^2 [c.f. Fig. 6(a)–(d)] and the separated configurations $(A^2B^1)^*$ and $(A^2B^2)^*$ [Fig. 6(e)–(f)]. The substitutional energies of V and Nb co-doped with other TMs are listed in Table 2 for all the considered configurations. It is clear that most of the adjacent configurations are energetically favored over the separated configurations, indicating a stronger interaction between TMs than between the TM and Mg atoms. As a unique case, it is noted that the energy of NbPd in the $(A^2B^2)^*$ configuration is slightly lower than that of NbPd in the A^2B^2 configuration, indicating that these configurations might be separated in the second layer.

The energy difference between the A^2B^1 and A^2B^2 co-doped Mg(0001) configurations is illustrated in Fig. 7 for each of the studied cases. In comparison to the single TM doping, the energy difference between the first and second layer doping is significantly reduced (to less than 0.1 eV) for Group B atoms

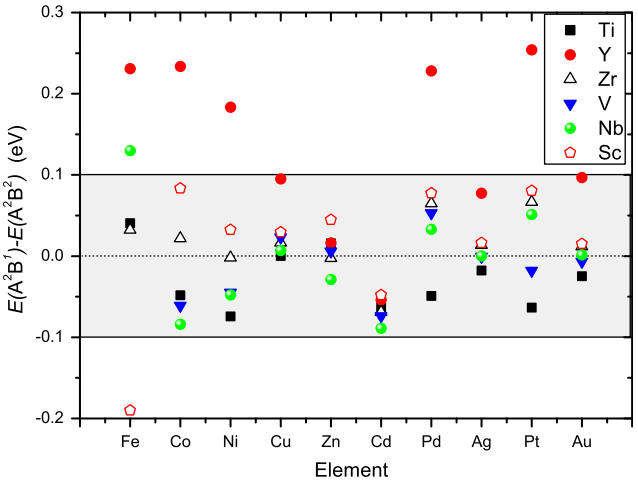

Fig. 7 – The energy difference between the A^2B^1 and A^2B^2 co-doped Mg(1000) configurations. Negative values indicate that atom B is energetically favorable in the first layer. Here, atoms A (A = Ti, Y, Zr, V, Nb) remain in the second layer (A^2), whereas atoms B are placed in the first (B^1) and second layers (B^2) adjacent to atom A. Black squares, red circles, open triangles, blue triangles, green circles, and open pentagons correspond to A = Ti, Y, Zr, V, Nb, and Sc, respectively (For interpretation of the references to color in this figure legend, the reader is referred to the web version of this article.)

when co-doped with Group A atoms except Y. Furthermore, most of Group A atoms are energetically favorable in the second layer when co-doped with Ti. In Group B, Co, and Ni, when co-doped with Ti, V, and Nb, are relatively easily stabilized in the first layer because their substitutional energies are significantly lower in the first layer than when the TMs are in the second layer. Finally, Fe, an example of an element not included in Group B, cannot be stabilized in the first layer when doped with Group A atoms other than Sc because of its strong preference to be in the second layer in single atom doping.

4. Conclusion

In summary, we have performed a systematic theoretical investigation of the stability of metal dopants and vacancies on Mg(0001) surfaces and the effect of this doping on hydrogen adsorption. All of the studied single TMs (corresponding to a low concentration) prefer to remain in the second layer, and their stabilities strongly correlate to their atomic radii and electronegativity. Additionally, the first layer TMs significantly enhance H adsorption with respect to a clean Mg(0001) surface, whereas the adsorption is comparable to that of the clean surface when the TMs are located in the second layer. Finally, when two different TMs are co-doped on a Mg(0001) surface, Ti acts as a good "assistant" that can stabilize co-doped Co, Ni, Pd, Ag, Pt, and Au in the first layers. Ni and Co are easily incorporated into the first layer of a Mg surface when co-doped with Ti, V, and Nb. This finding leads to a possible approach to stabilize the TM dopants in the first layer and, thus, benefits the design of advanced Mg-based hydrogen storage media.

Acknowledgments

This work was financially supported by MOST under project No. 2010CB631302 and by the Fundamental Research Funds for the Central Universities, SCUT, under projects 2009ZZ0068 and 2011ZG0017. The computing resources from the HPC Lab, Shenzhen Institute of Advanced Technology, Chinese Academy of Sciences (CAS), and from ScGrid of the Supercomputing Center, Computer Network Information Center of CAS, are gratefully acknowledged.

Appendix. Structural parameters, cohesive energies of metal bulk structures

We calculated the bulk structures of the elements Sc, Ti, V, Cr, Mn, Fe, Co, Ni, Cu, Zn, Y, Zr, Nb, Mo, Tc, Ru, Rh, Pd, Ag, Cd, Au, and Pt using $17 \times 17 \times 17$ and $19 \times 19 \times 15$ K-point grids for the primitive cells of cubic and hcp structures, respectively. The calculated structural parameters and cohesive energies are listed in Table 1 along with the electronegativities and atomic radii of the elements. All of the lattice parameters *a*, and *c* for hcp structures, are in agreement with experimental values and previous theoretical calculations [21]. According to our spin-polarized calculations, we conclude that the magnetic moments for Ni, Co, and Fe are 0.65, 1.63, and 2.20 μ_B/atom, respectively, which are in agreement with the corresponding experimental values of 0.61, 1.71 and 2.22 μ_B/atom [29]. The cohesive energies without zero-point vibrations for each element except Au and Co are close to the experimental values. For a better description of the cohesive energies of Au and Co, the relativistic effects (for Au) or GGA + U (for Co) should be considered according to Ref. [41]. It should be noted that we calculated the cohesive energy of Mn based on the structure from Ref.[42] because this structure is expected to be close to the experimental structure (see Ref. [43]), which has a complicated magnetic structure.

REFERENCES

[1] Jena P. Materials for hydrogen storage: past, present, and future. J Phys Chem Lett 2011;2:206–11.
[2] Schlapbach L, Zuttel A. Hydrogen-storage materials for mobile applications. Nature 2001;414:353–8.
[3] Stampfer JF, Holley CE, Suttle JF. The magnesium–hydrogen system. J Am Chem Soc 1960;82:3504–8.
[4] Huot J, Liang G, Boily S, Van Neste A, Schulz R. Structural study and hydrogen sorption kinetics of ball-milled magnesium hydride. J Alloy Compd 1999;295:495–500.
[5] Friedrichs O, Sanchez-Lopez JC, Lopez-Cartes C, Dornheim M, Klassen T, Bormann R, et al. Chemical and microstructural study of the oxygen passivation behaviour of nanocrystalline Mg and MgH_2. Appl Surf Sci 2006;252:2334–45.

[6] Johansson M, Ostenfeld CW, Chorkendorff I. Adsorption of hydrogen on clean and modified magnesium films. Phys Rev B 2006;74:193408.
[7] Friedlmeier G, Groll M. Experimental analysis and modelling of the hydriding kinetics of Ni-doped and pure Mg. J Alloy Compd 1997;253–254:550–5.
[8] Smith KC, Fisher TS, Waghmare UV, Grau-Crespo R. Dopant-vacancy binding effects in Li-doped magnesium hydride. Phys Rev B 2010;82:134109–18.
[9] Sakintuna B, Lamari-Darkrim F, Hirscher M. Metal hydride materials for solid hydrogen storage: a review. Int J Hydrogen Energy 2007;32:1121–40.
[10] Zaluska A, Zaluski L, Strom-Olsen JO. Nanocrystalline magnesium for hydrogen storage. J Alloy Compd 1999;288: 217–25.
[11] Liang G, Huot J, Boily S, Van Neste A, Schulz R. Catalytic effect of transition metals on hydrogen sorption in nanocrystalline ball milled MgH_2–Tm (Tm = Ti, V, Mn, Fe and Ni) systems. J Alloy Compd 1999;292:247–52.
[12] Gutfleisch O, Dal Toe S, Herrich M, Handstein A, Pratt A. Hydrogen sorption properties of Mg—1 wt.% Ni—0.2 wt.% Pd prepared by reactive milling. J Alloy Compd 2005;404:413–6.
[13] Molinas B, Ghilarducci AA, Melnichuk M, Corso HL, Peretti HA, Agresti F, et al. Scaled-up production of a promising Mg-based hydride for hydrogen storage. Int J Hydrogen Energy 2009;34:4597–601.
[14] Kalinichenka S, Rontzsch L, Kieback B. Structural and hydrogen storage properties of melt-spun Mg–Ni–Y alloys. Int J Hydrogen Energy 2009;34:7749–55.
[15] Jain IP, Lal C, Jain A. Hydrogen storage in Mg: a most promising material. Int J Hydrogen Energy 2010;35:5133–44.
[16] Patah A, Takasaki A, Szmyd JS. Influence of multiple oxide (Cr_2O_3/Nb_2O_5) addition on the sorption kinetics of MgH_2. Int J Hydrogen Energy 2009;34:3032–7.
[17] Du AJ, Smith SC, Yao XD, Lu GQ. First-principle study of adsorption of hydrogen on Ti-doped Mg(0001) surface. J Phys Chem B 2006;110:21747–50.
[18] Du AJ, Smith SC, Yao XD, Lu GQ. Hydrogen spillover mechanism on a Pd-doped Mg surface as revealed by ab initio density functional calculation. J Am Chem Soc 2007; 129:10201–4.
[19] Du AJ, Smith SC, Yao XD, Sun CH, Li L, Lu GQ. The role of V_2O_5 on the dehydrogenation and hydrogenation in magnesium hydride: an ab initio study. Appl Phys Lett 2008; 92:163106–9.
[20] Pozzo M, Alfe D, Amieiro A, French S, Pratt A. Hydrogen dissociation and diffusion on Ni- and Ti-doped Mg(0001) surfaces. J Chem Phys 2008;128:094703–11.
[21] Pozzo M, Alfe D. Hydrogen dissociation and diffusion on transition metal (=Ti, Zr, V, Fe, Ru, Co, Rh, Ni, Pd, Cu, Ag)-doped Mg(0001) surfaces. Int J Hydrogen Energy 2009;34:1922–30.
[22] Du AJ, Smith SC, Lu GQ. First-principle studies of the formation and diffusion of hydrogen vacancies in magnesium hydride. J Phys Chem C 2007;111:8360–5.
[23] Ismer L, Park MS, Janotti A, Van de Walle CG. Interactions between hydrogen impurities and vacancies in Mg and Al: a comparative analysis based on density functional theory. Phys Rev B 2009;80:184110.
[24] Banerjee S, Pillai CGS, Majumder C. First-principles study of the H_2 interaction with transition metal (Ti, V, Ni) doped Mg(0001) surface: implications for H-storage materials. J Chem Phys 2008;129:174703–6.
[25] Banerjee S, Pillai CGS, Majumder C. Dissociation and diffusion of hydrogen on the Mg(0001) surface: catalytic effect of V and Ni double substitution. J Phys Chem C 2009; 113:10574–9.
[26] Kresse G, Furthmuller J. Efficient iterative schemes for ab initio total-energy calculations using a plane-wave basis set. Phys Rev B 1996;54:11169–87.
[27] Perdew JP, Burke K, Ernzerhof M. Generalized gradient approximation made simple. Phys Rev Lett 1996;77:3865–9.
[28] Kresse G, Joubert D. From ultrasoft pseudopotentials to the projector augmented-wave method. Phys Rev B 1999;59: 1758–76.
[29] Kittel C. Introduction to solid state physics. 8th ed. New York: Wiley; 2005.
[30] Swanson HE, Morris MC, Evans EH, Ulmer L. Standard X-ray diffraction powder patterns. National Bureau of Standards 539; 1953. p. 1–95.
[31] Monkhorst HJ, Pack JD. Special points for Brillouin-zone integrations. Phys Rev B 1976;13:5188–93.
[32] Henkelman G, Arnaldsson A, Jonsson H. A fast and robust algorithm for Bader decomposition of charge density. Comput Mater Sci 2006;36:354–60.
[33] Sanville E, Kenny SD, Smith R, Henkelman G. Improved grid-based algorithm for Bader charge allocation. J Comput Chem 2007;28:899–908.
[34] Checchetto R, Bazzanella N, Miotello A. Nb clusters formation in Nb-doped magnesium hydride. Appl Phys Lett 2005;87.
[35] Sprunger PT, Plummer EW. Interaction of hydrogen with the Ag(110) surface. Phys Rev B 1993;48:14436–48.
[36] Geunseop L, Plummer EW. Interaction of hydrogen with the Ag(111) surface. Phys Rev B Condens Matter 1995;51:7250–61.
[37] Stobinski L, Dus R. Atomic hydrogen adsorption on thin gold films. Surf Sci 1992;269–270:383–8.
[38] Liang G, Schulz R. The reaction of hydrogen with Mg–Cd alloys prepared by mechanical alloying. J Mater Sci 2004;39: 1557–62.
[39] Vegge T, Hedegaard-Jensen LS, Bonde J, Munter TR, Norskov JK. Trends in hydride formation energies for magnesium-3d transition metal alloys. J Alloy Compd 2005;386:1–7.
[40] Aguey-Zinsou KF, Ares-Fernandez JR. Hydrogen in magnesium: new perspectives toward functional stores. Energy Environ Sci 2010;3:526–43.
[41] O'Shea VAD, Moreira IDR, Roldan A, Illas F. Electronic and magnetic structure of bulk cobalt: the alpha, beta, and epsilon-phases from density functional theory calculations. J Chem Phys 2010;133.
[42] Haglund J, Fernandez Guillermet A, Grimvall G, Korling M. Theory of bonding in transition-metal carbides and nitrides. Phys Rev B 1993;48:11685.
[43] Hobbs D, Hafner J, Spišák D. Understanding the complex metallic element Mn. I. Crystalline and noncollinear magnetic structure of alpha-Mn. Phys Rev B 2003;68:014407.
[44] Bailar JC, Emeleus HJ, Nyholm S, Trotman-Dickenson AF. Comprehensive inorganic chemistry. Oxford: Pergamon Press; 1973.
[45] Chandra S. Comprehensive inorganic chemistry, vol. II. New Delhi: New Age International; 2006.